Broken Screw Rotational Symmetry in the Near-Surface Electronic Structure of *AB*-Stacked Crystals

Hiroaki Tanaka,[1] Shota Okazaki,[2] Masaru Kobayashi,[2] Yuto Fukushima,[1] Yosuke Arai,[1] Takushi Iimori,[1] Mikk Lippmaa,[1] Kohei Yamagami,[3] Yoshinori Kotani,[3] Fumio Komori,[4] Kenta Kuroda,[5,6,*] Takao Sasagawa,[2,†] and Takeshi Kondo[1,7,‡]

[1]*Institute for Solid State Physics, The University of Tokyo, Kashiwa, Chiba 277-8581, Japan*
[2]*Materials and Structures Laboratory, Tokyo Institute of Technology, Yokohama, Kanagawa 226-8503, Japan*
[3]*Japan Synchrotron Radiation Research Institute (JASRI), Sayo, Hyogo 679-5198, Japan*
[4]*Institute of Industrial Science, The University of Tokyo, Meguro-ku, Tokyo 153-8505, Japan*
[5]*Graduate School of Advanced Science and Engineering, Hiroshima University, Higashi-hiroshima, Hiroshima 739-8526, Japan*
[6]*International Institute for Sustainability with Knotted Chiral Meta Matter (WPI-SKCM^2), Higashi-hiroshima, Hiroshima 739-8526, Japan*
[7]*Trans-scale Quantum Science Institute, The University of Tokyo, Bunkyo-ku, Tokyo 113-0033, Japan*

(Received 2 August 2023; revised 29 November 2023; accepted 22 February 2024; published 29 March 2024)

We investigate the electronic structure of $2H$-NbS_2 and h-BN by angle-resolved photoemission spectroscopy (ARPES) and photoemission intensity calculations. Although in bulk form, these materials are expected to exhibit band degeneracy in the $k_z = \pi/c$ plane due to screw rotation and time-reversal symmetries, we observe gapped band dispersion near the surface. We extract from first-principles calculations the near-surface electronic structure probed by ARPES and find that the calculated photoemission spectra from the near-surface region reproduce the gapped ARPES spectra. Our results show that the near-surface electronic structure can be qualitatively different from the bulk electronic structure due to partially broken nonsymmorphic symmetries.

DOI: 10.1103/PhysRevLett.132.136402

Nonsymmorphic symmetries, such as screw rotations and glide reflections, can induce characteristic degeneracies in the band dispersions of crystals. One such degeneracy is a nodal surface that is stabilized by a combination of a 2_1 screw rotation with time-reversal symmetry. If spin-orbit coupling (SOC) can be ignored, these two symmetries lead to degenerate band pairs at Brillouin zone boundary surfaces [1]. A gap can form at such nodal planes in the presence of SOC, but the band degeneracy is partially protected by the nonsymmorphic symmetries, forming nodal lines [2–4]. Recent studies have shown that such nodal line materials can exhibit extremely large magnetoresistance [5–7] and other emergent properties, raising the prospect of device applications.

Furthermore, since the nonsymmorphic symmetries responsible for the formation of the nodal lines may not be maintained in the surface region, the electronic structure near the surface may differ from the bulk electronic structure. For example, a nodal line material ZrSiS has been reported to exhibit surface-specific states [8]. Angle-resolved photoemission spectroscopy (ARPES) is a suitable probe for investigating the near-surface electronic structure because its probing depth is up to a few nanometers from the surface due to electron scattering processes [9]. In addition, it has been unclear whether bulk band degeneracy due to nonsymmorphic symmetries can be retained in the near-surface region. While multifold degeneracy has been observed by ARPES in nonsymmorphic CoSi [10,11], no degeneracy was observed in a nodal line material $2H$-NbS_2 [12]. Clearly, more detailed experiments and calculations are needed to interpret the ARPES results of nonsymmorphic materials.

In this Letter, we present an extensive soft-x-ray (SX) ARPES study of the differences between the near-surface electronic structure and the bulk structure hosting nodal lines. We examine the near-surface electronic structure of *AB*-stacked $2H$-NbS_2 and h-BN (space group $P6_3/mmc$) crystals, both of which host bulk nodal lines on the $k_z = \pi/c$ plane. Since h-BN is a wide-gap semiconductor, we used thin flakes of h-BN to avoid charge up during ARPES measurements. Although ARPES measurements of h-BN flakes are technically difficult, we chose h-BN because fewer valence electrons in h-BN compared to $2H$-NbS_2 make the spectrum analysis easier and give more comprehensive evidence. We found gapped band dispersions on the $k_z = \pi/c$ plane, indicating that the broken screw rotational symmetry at the surface opens an energy gap in the near-surface electronic structure. Such band splitting cannot be explained by the k_z-broadening effect with the typical length scale $\Delta k_z = 0.1$ Å^{-1} [13], which has been frequently employed to discuss the surface sensitivity of ARPES. Taking into account the surface sensitivity, our photoemission intensity calculations could reproduce such gapped spectra by adjusting the probing depth parameter in the simulation. Our results show that incomplete

nonsymmorphic symmetries can alter the near-surface electronic structure associated with the bulk nodal lines, not only inducing emergent surface states as previously reported [8].

Single crystals of $2H$-NbS_2 were grown by the chemical vapor transport method, as explained in an earlier report [12]. Single crystals of h-BN were grown by the flux method under atmospheric pressure; information on crystal growth and characterization is in the Supplemental Material Note 1 [14]. SX-ARPES measurements were performed at BL25SU of SPring-8 [15], using 370–760 eV SX light. The measurement temperature was kept at around 50 K, and the energy resolution was ≈80 meV. Since $2H$-NbS_2 is a metal with sufficient conductivity, we cleaved as-grown samples *in situ* in an ultrahigh vacuum better than $\sim 3 \times 10^{-8}$ Pa to obtain clean surfaces. On the other hand, special care was taken in the preparation of h-BN to avoid charge up. We used thin exfoliated flakes of h-BN to reduce the resistance between the substrate and the top surface of the sample. Note 1 in [14] explains the detailed procedure of the flake fabrication and the dry pickup method of sample mounting in the ARPES chamber [16,17]. The h-BN flakes were several tens of micrometers wide and a few hundred nanometers thick (Fig. S2 in [14]). Since these samples are much smaller than typical as-grown crystals, we used micrometer-focused SX [15]. In the photoemission intensity calculations, we used OpenMX [18] and a recently developed photoemission angular distribution simulator SPADExp [19]. Note 2 in [14] summarizes the calculation conditions.

We start our discussion with SX-ARPES results of $2H$-NbS_2. While a previous study has already reported the gapped band dispersion at the L points [12], we performed SX-ARPES measurements over a wider k_z range to check the universality of this phenomenon. The AL path is suitable for our discussion because the crystal symmetry prohibits the gap opening due to SOC (Fig. S4(a) in [14]). Figure 1(c) clearly shows that one paired band at the valence band top has an energy gap of about 0.5 eV at the L point. On the other hand, the bulk band dispersion at the L point exhibits symmetry-related degeneracy [Fig. 1(d)]; a small energy gap at the momentum points other than the L point is due to the curved momentum path in single-photon-energy ARPES measurements [Fig. 1(b)]. The k_z dispersion along the ML line, taken by changing the photon energy from 370 to 750 eV, also shows gapped dispersion at all observed L points [Fig. 1(e)]. These results clearly show that the bulk band degeneracy caused by the screw rotational symmetry is broken in the near-surface electronic structure of $2H$-NbS_2.

Next, we investigated the electronic structure of h-BN [Fig. 2(a)]. As was noted earlier, ARPES spectra of h-BN were easier to discuss due to fewer valence electrons in this material. The use of the micrometer-focused SX beam ensured that the photoemission spectra were derived only from the h-BN flakes. We observed the constant-energy

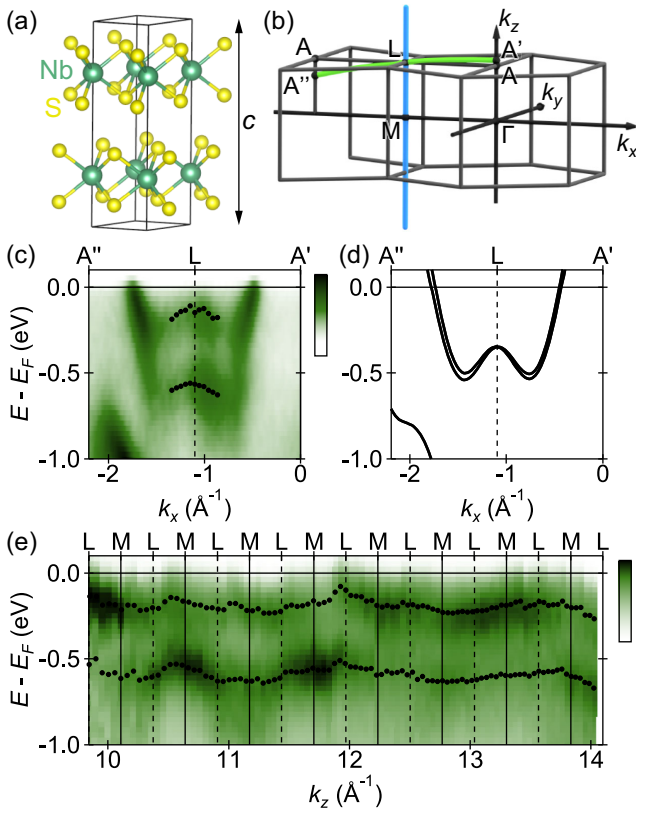

FIG. 1. Band dispersion of $2H$-NbS_2. (a) Crystal structure. The unit cell height is $c = 11.89$ Å. (b) The Brillouin zone of a hexagonal crystal with high-symmetry point labels. The blue and green curves represent momentum paths along which the band dispersions are presented. The green curve corresponds to the momentum path in single-photon-energy ARPES measurements. (c) Band dispersion along the green curve taken with 525 eV SX light. The L point is on the $k_z = 22.5 \times 2\pi/c$ plane. (d) Bulk band dispersion calculated along the same path as (c). (e) k_z dispersion along the blue ML path. In (c) and (e) the black dots represent the band positions determined by fitting the energy distribution curves [Figs. S4(b) and S4(c) in [14], respectively].

surface [Fig. 2(b)], which coincided well with a previous ARPES study of h-BN with submicrometer-focused vacuum ultraviolet (VUV) light [20], and signal from the substrate was negligible. The core-level spectra clearly exhibited the $1s$ peaks of boron and nitrogen only when the soft-x-ray beam was on the h-BN flake (Fig. S5 in [14]). The band dispersion around the L point has an energy gap of about 0.8 eV [Figs. 2(c) and 2(h)], contrary to the gapless bulk band dispersion [Fig. 2(d)]. Such inconsistent behavior between experiment and bulk band calculations is similar to our SX-ARPES results of $2H$-NbS_2 (Fig. 1).

Because of negligible SOC and fewer electrons, we could examine the degeneracy of the h-BN π band along the entire AL path. We found that the ARPES behavior at the A point differed from that at the L point.

First, we observed only a single peak in the energy distribution curve extracted along the ΓA path (Fig. S6(a)

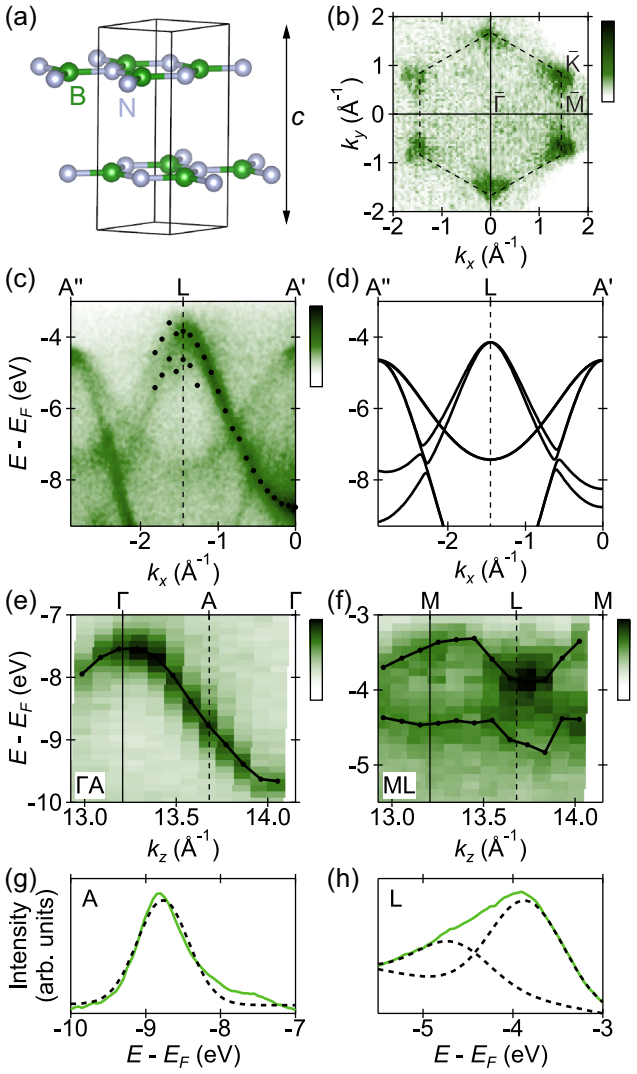

FIG. 2. Band dispersion of h-BN. (a) Crystal structure. The unit cell height is $c = 6.66$ Å. (b) Constant-energy surface at $E_F - 3$ eV taken with 750 eV SX light. The dashed hexagon represents the Brillouin zone. (c) Band dispersion crossing the L point taken with 720 eV SX light. The L point is on the $k_z = 14.5 \times 2\pi/c$ plane. (d) Bulk band dispersion along the same path as (c). (e),(f) k_z dispersions along the ΓA and ML paths, respectively. In (c), (e), and (f) the black dots and solid curves represent band positions determined by fitting the energy distribution curves [Figs. S7, S6(a), and S6(g) in [14], respectively]. (g),(h) Energy distribution curves at the A and L points, respectively. The black dashed curves represent the peaks included in the fitting function.

in [14]). Since the peak profiles are symmetric and fit well with a single Gaussian, they can be assigned to a single band. As a result, the k_z dispersion of the π band along the ΓA direction shows only a single oscillating dispersion profile, while the other dispersion forming a pair is absent [Fig. 2(e)]. Such a phenomenon has been frequently observed in the k_z dispersion of AB-stacked materials [12,21,22]. If the A and B layers are similar, the electronic structure of the crystal can be approximated by a system with a height of $c/2$ containing only one layer. The approximated electronic structure gives a single band with a periodicity of $2\pi/(c/2) = 4\pi/c$. We reproduced the $4\pi/c$ dispersion in the photoemission intensity calculations of the h-BN bulk (Fig. S10 in [14]).

Second, more importantly, the k_z dispersion along the ΓA path has no energy gap at the A point [Figs. 2(e) and 2(g)]. This behavior differs from the dispersion along the ML path [Figs. 2(f) and 2(h)] and that of $2H$-NbS_2 [Fig. 1(e)] but is consistent with ARPES study of graphite [22], which has a similar crystal structure to h-BN. With increasing k_x value from the ΓA to ML paths, we observed a crossover from the gapless "bulk" spectra to the gapped "surface" spectra (Note 5 in [14]). This crossover direction is physically reasonable; a nonzero k_x component means that the photoelectron momentum vector is canted away from the surface normal, making the effective distance to the surface longer and the measurement more surface sensitive. To summarize, ARPES spectra and bulk band dispersion can be substantially different at least partially, even if we perform relatively bulk-sensitive soft-x-ray ARPES [9]. The deviation has been discussed as the k_z-broadening effect in the reciprocal space. While it can explain the peak position shift [23] and may cause the band splitting, our k_z-broadening simulation revealed that the typical broadening length scale $\Delta k_z = 0.1$ Å^{-1} [13] was insufficient to cause the band splitting (Note 6 in [14]).

To elucidate the mechanism that leads to the gapped surface spectra, we performed photoemission intensity calculations taking into account the surface sensitivity of ARPES in real space. The first-principles calculations of h-BN were done using a 40-bilayer slab to obtain the near-surface electronic structure. However, the band dispersion includes the whole electronic structure of the slab and is very broad [Fig. 3(a)]. We, therefore, performed photoemission intensity calculations to obtain the matrix element between the initial and final states and extract the near-surface electronic structure [24]. The initial state is a ground state wave function obtained by first-principles calculations, and the final state is a plane wave with decay due to scattering. Combining the large slab system and final states with decay enables the photoemission simulation to extract the near-surface electronic structure observed by ARPES [19]. If the decayed final states cover a sufficient number of unit cells along the z direction, we can expect a bulk spectrum shaped by the momentum selection rule. Otherwise, the calculated spectra will deviate from the bulk spectrum, resulting in a gapped surface spectrum [Fig. 3(a)], as mainly observed in our ARPES measurements. From this consideration, we can claim that the band splitting due to the broken nonsymmorphic symmetry is smaller than the band width along the k_z direction.

We compared two functions for the square of decay related to the photoelectron emission probability $p(z)$: an

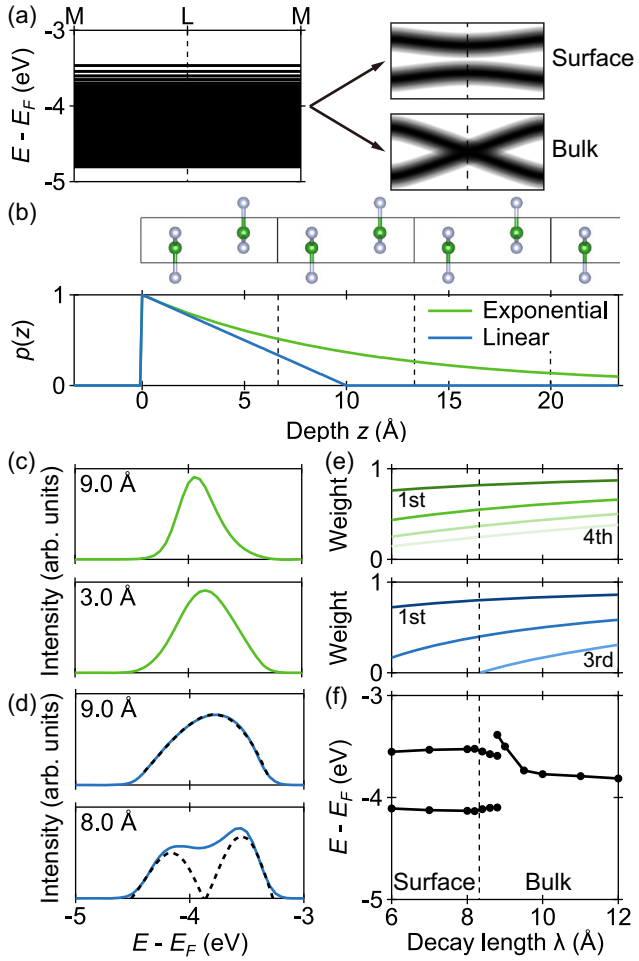

FIG. 3. Photoemission intensity calculations of h-BN. (a) Calculated slab band dispersion along the ML path and schematic surface and bulk spectra obtained by successive photoemission intensity calculations. (b) Exponential and linear decay functions, where the depth parameter λ is set to 10 Å. The dashed grid corresponds to the height of the unit cell, as drawn in the top panel. (c),(d) Calculated spectra at the L point using the exponential and linear decay functions with different λ values, respectively. In (d) the black dashed curves represent the peaks included in the fitting function. (e) λ dependence of the decay strength at each atomic layer position for both exponential and linear functions. (f) λ dependence of peak positions extracted from calculated spectra using the linear decay function (Fig. S11 in [14]). In (e) and (f) the dashed vertical lines represent the third layer position.

exponential function $\exp(-z/\lambda)$ and a linear function $\max(1-z/\lambda, 0)$ [Fig. 3(b)]. Exponential depth decay has been commonly used in discussing the surface sensitivity of ARPES [24] based on the inelastic scattering measurements of photoelectrons from polycrystalline films [25,26]. However, it did not reproduce the gapped surface spectra even for unreasonably small mean free path parameter $\lambda = 3$ Å [Fig. 3(c)]. The gapless spectrum at $\lambda = 3$ Å is consistent with our k_z-broadening simulation ($\Delta k_z = 0.6\pi/c$) exhibiting band position shift but preserved band degeneracy (Fig. S9(c) in [14]). The disagreement between experiments and simulations may be because the exponential decay is too slow to reproduce the ARPES spectra, where both the inelastic and elastic scatterings matter. Therefore, instead of the exponential decay, we employed the linear decay function, which is steeper than exponential and has the cutoff property. The steeper decay function can be interpreted as a different peak shape than what has been used before in the context of the k_z-broadening effect [23]. The linear decay function is appropriate for comprehensive discussion because it is controlled only by one continuous parameter λ. Using the linear decay function, we reproduced the gapped surface spectra that could be fitted well with two Gaussians when $\lambda < 8.8$ Å [Fig. 3(d)]. The crossover from a single to a double peak spectrum happens abruptly (Fig. S11 in [14]), and the position where the change occurs seems to be related to the third layer from the surface. Figures 3(e) and 3(f) show that when we increase the depth parameter λ, the surface spectra abruptly change to the bulk shape as the decay function starts to cover the third layer, marked with the dashed vertical line in the figures. The exponential decay function, therefore, always produced a gapless bulk spectrum due to the long decay tail that covers deeper layers, even if λ is quite small [Fig. 3(e) top panel]. While the linear decay function successfully reproduced gapped spectra, the decay shape is empirical. We hope further research will discover the decay function shape due to inelastic and elastic scattering by calculations and/or experiments.

Finally, we performed photoemission angular distribution calculations for h-BN to validate the SX-ARPES results (Fig. 2). The calculated photoemission spectra around the L point, using a linear decay function with $\lambda = 8$ Å, shows an energy gap [Fig. 4(a)] that is very similar to the experimental observation [Fig. 2(c)]. On the other hand, using just a slightly larger decay parameter of $\lambda = 12$ Å produces a gapless dispersion curve [Fig. 4(b)], agreeing well with the experimental data around the A point. The k_z dispersions along the ML and ΓA paths reproduce the gapped and gapless behaviors [Figs. 4(c) and 4(d)] when an appropriate decay parameter is chosen. These results indicate that the out-of-plane scattering length slightly depends on the in-plane momentum of a photoelectron, even for the same π band. This assumption is reasonable because the negative correlation between the in-plane momentum and the scattering length is physically natural, as explained earlier in the paragraph on h-BN experiments, and the scattering length difference needed to explain the different experimental spectra is not large. In addition, the nonuniform electronic structure in single crystals may enhance the angle dependence of the scattering phenomena.

Additionally, the decay conditions used in the h-BN calculations succeeded in reproducing the gapped surface

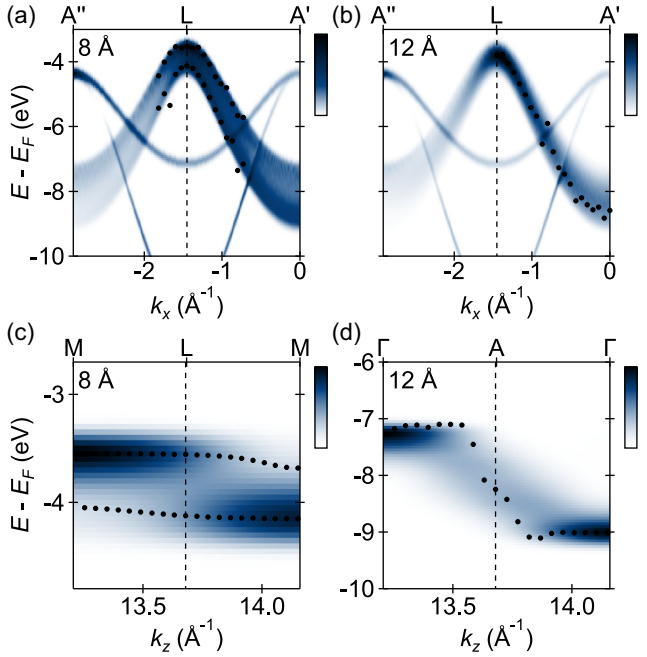

FIG. 4. Photoemission angular distribution calculations of h-BN. (a),(b) Calculated band dispersions along the path crossing the L point. (c),(d) Calculated band dispersions along the ML and ΓA paths, respectively. The left top labels represent the linear decay parameter λ. The black dots in the panels represent peak positions determined by fitting the energy distribution curves (Figs. S12 and S13 in [14]).

spectra of $2H$-NbS_2 (Fig. S14 in [14]). Since the third layer of $2H$-NbS_2 is deeper than h-BN, the photoemission spectra are always gapped, independent of the selection of the decay length parameter. We can exclude the possibility of an SOC-derived energy gap because the gap behavior is independent of the inclusion of SOC. Our results indicate that photoemission intensity simulations using a linear decay function can be universally applicable to other materials because the photoelectron inelastic mean free path exhibits a universal energy dependence [9]. In addition, our λ dependence analysis of the simulated spectra gives insight into previous observations of multifold degeneracy in nonsymmorphic CoSi [10,11] and Dirac points in Na_3Bi [27]. Since CoSi has a three-dimensional structure, which can be interpreted as a stacked material composed of very thin layers, more layers are included within the ARPES probing depth than in the case of quasi-two-dimensional $2H$-NbS_2 and h-BN. Considering our discussion that the number of layers included in the probing depth is essential to determine the appearance of bulk degeneracy in ARPES spectra, three-dimensional nonsymmorphic materials seem to be more likely to exhibit bulk band degeneracy in ARPES experiments. On the other hand, since the Dirac points in Na_3Bi are protected by in-plane rotational symmetry, their degeneracy will be conserved in the near-surface electronic structure, consistent with the clear observation of the Dirac points by ARPES [27]. Nevertheless, another possibility is that their observed degeneracy can be decomposed into several peaks if the energy distribution curve is analyzed in more detail, as we did in the present study. In addition, since the observed degeneracies discussed previously are located near the Fermi level, other peak structures may exist above the Fermi level and therefore be absent in experimental spectra.

In conclusion, we investigated the symmetry-protected band degeneracy in $2H$-NbS_2 and h-BN by ARPES and photoemission intensity calculations. While the bulk band degeneracy in these materials is due to the coexistence of 2_1 screw rotation and time-reversal symmetries, the near-surface electronic structure that ARPES can probe may differ from the bulk because the screw rotation symmetry is broken at the surface. Indeed, we observed gapped band dispersion on the $k_z = \pi/c$ plane in most cases other than around the A point of h-BN. Our photoemission intensity calculations to extract the near-surface electronic structure revealed that the assumption of exponential photoemission probability decay, which has been frequently used to discuss the surface sensitivity of ARPES, cannot reproduce the experimental results. Instead, a steeper linear decay reproduced the gapped behavior with an abrupt crossover to gapless bulk spectra when the decay length parameter was increased, giving a reasonable explanation for the simultaneous observation of surface and bulk spectra at the L and A points of h-BN. This work demonstrates the necessity to consider the surface electronic structure to discuss photoemission spectra, even in relatively bulk-sensitive SX-ARPES. Furthermore, we show that the electronic structure in the near-surface region can deviate significantly from the symmetry-protected bulk electronic structure, providing a possibility of a more exotic electronic structure in the surface or interface of nodal line materials.

We thank Abdelkarim Ouerghi for providing their experimental methods of VUV-ARPES measurements of h-BN [20] and Haruki Watanabe for theoretical advice. This work was also supported by Grant-in-Aid for JSPS Fellows (Grant No. JP21J20657), Grant-in-Aid for Scientific Research on Innovative Areas (Grants No. JP21H05236 and No. JP22H04483), Grant-in-Aid for Challenging Research (Pioneering) (Grants No. JP21K18181 and No. JP23K17351), Grant-in-Aid for Scientific Research (B) (Grant No. JP22H01943), Grant-in-Aid for Scientific Research (A) (Grants No. JP21H04652 and No. JP21H04439), Japan Science and Technology Agency (JST) (Grant No. JPMJMI21G2), Quantum Leap Flagship Program from Ministry of Education, Culture, Sports, Science and Technology (MEXT Q-LEAP) (Grant No. JPMXS0118068681), the Asahi Glass Foundation, the Murata Science Foundation, and Photon and Quantum Basic Research Coordinated Development Program from MEXT. Optical microscope measurements were performed using the facilities of the Materials Design and

Characterization Laboratory in the Institute for Solid State Physics, the University of Tokyo. The synchrotron radiation experiments were performed with the approval of Japan Synchrotron Radiation Research Institute (JASRI) (Proposals No. 2020A1181, No. 2021A1259, No. 2021B1797, and No. 2022A1687).

*kuroken224@hiroshima-u.ac.jp
†sasagawa@msl.titech.ac.jp
‡kondo1215@issp.u-tokyo.ac.jp

[1] G. Chang, B. J. Wieder, F. Schindler, D. S. Sanchez, I. Belopolski, S.-M. Huang, B. Singh, D. Wu, T.-R. Chang, T. Neupert, S.-Y. Xu, H. Lin, and M. Z. Hasan, Nat. Mater. **17**, 978 (2018).
[2] Q.-F. Liang, J. Zhou, R. Yu, Z. Wang, and H. Weng, Phys. Rev. B **93**, 085427 (2016).
[3] L. M. Schoop, M. N. Ali, C. Straßer, A. Topp, A. Varykhalov, D. Marchenko, V. Duppel, S. S. P. Parkin, B. V. Lotsch, and C. R. Ast, Nat. Commun. **7**, 11696 (2016).
[4] K. Funada, A. Yamakage, N. Yamashina, and H. Kageyama, J. Phys. Soc. Jpn. **88**, 044711 (2019).
[5] Y.-Y. Lv, B.-B. Zhang, X. Li, S.-H. Yao, Y. B. Chen, J. Zhou, S.-T. Zhang, M.-H. Lu, and Y.-F. Chen, Appl. Phys. Lett. **108**, 244101 (2016).
[6] M. N. Ali, L. M. Schoop, C. Garg, J. M. Lippmann, E. Lara, B. Lotsch, and S. S. P. Parkin, Sci. Adv. **2**, e1601742 (2016).
[7] R. Singha, A. K. Pariari, B. Satpati, and P. Mandal, Proc. Natl. Acad. Sci. U.S.A. **114**, 2468 (2017).
[8] A. Topp, R. Queiroz, A. Grüneis, L. Müchler, A. W. Rost, A. Varykhalov, D. Marchenko, M. Krivenkov, F. Rodolakis, J. L. McChesney, B. V. Lotsch, L. M. Schoop, and C. R. Ast, Phys. Rev. X **7**, 041073 (2017).
[9] M. P. Seah and W. A. Dench, Surf. Interface Anal. **1**, 2 (1979).
[10] D. Takane, Z. Wang, S. Souma, K. Nakayama, T. Nakamura, H. Oinuma, Y. Nakata, H. Iwasawa, C. Cacho, T. Kim, K. Horiba, H. Kumigashira, T. Takahashi, Y. Ando, and T. Sato, Phys. Rev. Lett. **122**, 076402 (2019).
[11] Z. Rao, H. Li, T. Zhang, S. Tian, C. Li, B. Fu, C. Tang, L. Wang, Z. Li, W. Fan, J. Li, Y. Huang, Z. Liu, Y. Long, C. Fang, H. Weng, Y. Shi, H. Lei, Y. Sun, T. Qian, and H. Ding, Nature (London) **567**, 496 (2019).
[12] H. Tanaka, S. Okazaki, K. Kuroda, R. Noguchi, Y. Arai, S. Minami, S. Ideta, K. Tanaka, D. Lu, M. Hashimoto, V. Kandyba, M. Cattelan, A. Barinov, T. Muro, T. Sasagawa, and T. Kondo, Phys. Rev. B **105**, L121102 (2022).
[13] J. A. Sobota, Y. He, and Z.-X. Shen, Rev. Mod. Phys. **93**, 025006 (2021).
[14] See Supplemental Material at http://link.aps.org/supplemental/10.1103/PhysRevLett.132.136402 for the sample preparation and calculation methods and additional data supporting our arguments.
[15] T. Muro, Y. Senba, H. Ohashi, T. Ohkochi, T. Matsushita, T. Kinoshita, and S. Shin, J. Synchrotron Radiat. **28**, 1631 (2021).
[16] I. Cucchi, I. Gutiérrez-Lezama, E. Cappelli, S. McKeown Walker, F. Y. Bruno, G. Tenasini, L. Wang, N. Ubrig, C. Barreteau, E. Giannini, M. Gibertini, A. Tamai, A. F. Morpurgo, and F. Baumberger, Nano Lett. **19**, 554 (2019).
[17] S. Masubuchi, M. Sakano, Y. Tanaka, Y. Wakafuji, T. Yamamoto, S. Okazaki, K. Watanabe, T. Taniguchi, J. Li, H. Ejima, T. Sasagawa, K. Ishizaka, and T. Machida, Sci. Rep. **12**, 10936 (2022).
[18] T. Ozaki, Phys. Rev. B **67**, 155108 (2003).
[19] H. Tanaka, K. Kuroda, and T. Matsushita, J. Electron Spectrosc. Relat. Phenom. **264**, 147297 (2023).
[20] H. Henck, D. Pierucci, G. Fugallo, J. Avila, G. Cassabois, Y. J. Dappe, M. G. Silly, C. Chen, B. Gil, M. Gatti, F. Sottile, F. Sirotti, M. C. Asensio, and A. Ouerghi, Phys. Rev. B **95**, 085410 (2017).
[21] D. Di Sante, P. K. Das, C. Bigi, Z. Ergönenc, N. Gürtler, J. A. Krieger, T. Schmitt, M. N. Ali, G. Rossi, R. Thomale, C. Franchini, S. Picozzi, J. Fujii, V. N. Strocov, G. Sangiovanni, I. Vobornik, R. J. Cava, and G. Panaccione, Phys. Rev. Lett. **119**, 026403 (2017).
[22] F. Matsui, H. Nishikawa, H. Daimon, M. Muntwiler, M. Takizawa, H. Namba, and T. Greber, Phys. Rev. B **97**, 045430 (2018).
[23] V. Strocov, J. Electron Spectrosc. Relat. Phenom. **130**, 65 (2003).
[24] S. Moser, J. Electron Spectrosc. Relat. Phenom. **214**, 29 (2017).
[25] H. Kanter, Phys. Rev. B **1**, 522 (1970).
[26] M. Klasson, J. Hedman, A. Berndtsson, R. Nilsson, C. Nordling, and P. Melnik, Phys. Scr. **5**, 93 (1972).
[27] Z. K. Liu, B. Zhou, Y. Zhang, Z. J. Wang, H. M. Weng, D. Prabhakaran, S.-K. Mo, Z. X. Shen, Z. Fang, X. Dai, Z. Hussain, and Y. L. Chen, Science **343**, 864 (2014).